Influence of Na-related defects on DUV nonlinear absorption in CaF_2: Nanosecond versus femtosecond laser pulses

Ch. Mühlig*[a], H. Stafast[a], W. Triebel[a], Th. Zeuner[a], Ch. Karras[a], M. Letz[b]
[a]Institute of Photonic Technology, Albert-Einstein-Str. 9, 07745 Jena, Germany;
[b]SCHOTT AG Research and Technology Development, Hattenbergstr. 10, 55122 Mainz, Germany

ABSTRACT

The influence of Na stabilized F and M centers on the DUV absorption behavior of CaF_2 is comparatively studied for nanosecond and femtosecond laser pulses by in-situ transmission and laser induced fluorescence measurements.
For 193 nm nanosecond pulses the steady state transmission of ArF laser pulses through CaF_2 is measured in dependence on the incident fluence $H \leq 10$ mJ cm^{-2} $pulse^{-1}$. The related absorption coefficients $\alpha^{st}(H)$ are proportional to H and rationalized by effective 1- and 2-photon absorption coefficients α^{eff} and β^{eff}, respectively. The α^{eff} and β^{eff} values increase with the Na content of the CaF_2 samples as identified by the fluorescence of Na related M_{Na} centers at 740 nm. This relation is simulated by a complex rate equation model describing the ArF laser induced M_{Na} generation and annealing. M_{Na} generation starts with intrinsic 2-photon absorption in CaF_2 yielding self-trapped excitons (STE). These pairs of F and H centers can separate upon thermal activation and the F centers combine with F_{Na} to form M_{Na} centers. M_{Na} annealing occurs by its photo dissociation into a pair of F and F_{Na} centers.
Comparative transmission measurements with DUV femtosecond pulses are done using the fourth harmonic of a Ti:Sa-fs-laser at 197 nm. The resulting β^{eff} values virtually show no dependence on the M_{Na} center concentration. Furthermore, the absolute β^{eff} values are lower by a factor of three compared to those obtained for nanosecond pulses. This is explained by additional two-step absorption for nanosecond pulses after formation of self-trapped excitons (STE).

Keywords: DUV femtosecond and nanosecond laser pulses, defect generation and annealing, nonlinear absorption, CaF_2

1. INTRODUCTION

Crystalline calcium fluoride (CaF_2) with its excellent transmission over a wide wavelength range is one material of choice for optics exposed to high intensity DUV laser light e.g. laser windows and optics in laser lithography. Furthermore, its high thermal conductivity makes it a promising host material for high power lasers in the near infrared region[1].
The ability of the CaF_2 crystal lattice to accept impurities is a large benefit for the growth of laser active materials like Yb:CaF_2 but it is also a drawback when CaF_2 of highest purity is needed for high power laser optics. Earlier investigations have shown, that even high purity CaF_2 can suffer from a considerable transmission decrease[2-4]. Therefore, it is necessary to clarify how residual impurities or defects of CaF_2 affect its durability under intense laser irradiation. Recently, the influence of sodium (Na) or yttrium (Y) on the ArF laser induced absorption was investigated[5,6]. Furthermore, several emission bands caused by trace impurities or structural defects were found[7]. Qualitative correlations between particular emission bands and the material's transmission properties were obtained[2,3].
In this work, ArF laser (nanosecond pulses) transmission and fluorescence measurements are applied to quantitatively investigate the influence of Na^+ stabilized M centers (M_{Na}) on the steady state absorption by CaF_2. The influence is quantified by effective 1- and 2-photon absorption coefficients which reflect the density of M_{Na} centers. The M_{Na} centers are generated and annealed by ArF laser irradiation.
Furthermore, transmission measurements are carried out using femtosecond DUV laser pulses and the obtained 2-photon absorption coefficients are compared to those obtained by nanosecond pulses of similar wavelength. The introduced model describing the ArF laser induced M_{Na} generation and annealing is taken to explain the different results obtained by nanosecond and femtosecond laser pulses.

*christian.muehlig@ipht-jena.de; phone +49 3641 206433; fax +49 3641 206499; www.ipht-jena.de

2. EXPERIMENTAL METHODS

A large number of CaF_2 samples (25 x 25 x 100 mm^3) showing different intensities of the characteristic fluorescence emission of M_{Na} centers at 620 and 740 nm[8,9] (Fig. 1) are investigated by ArF laser transmission measurements. In addition 6 CaF_2 samples of highest purity without any emission at 620 and 740 nm are selected as reference.

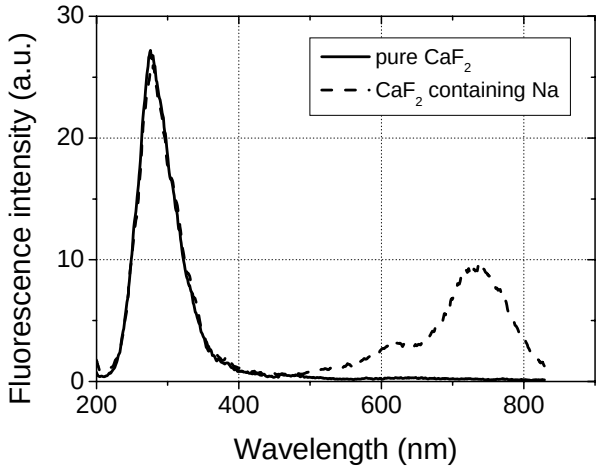

Figure 1: Fluorescence emission spectra of CaF_2 samples showing the intrinsic emission of self-trapped excitons (STE) only (solid line) and with additional bands at 620 and 740 nm due to Na related M_{Na} defect centers (broken line)

The experiments are carried out at room temperature in a nitrogen purged experimental setup using an ArF laser (LPX 240i, Lambda Physik) emitting pulses of $\tau_L \approx 30$ ns duration (second moment)[10]. The laser beam is shaped by an aperture in front of the sample to a cross section of 15 x 5 mm^2 with a top-hat like intensity profile. Prior to laser irradiation the relevant polished sample surfaces are cleaned with pure ethanol. *In situ* ArF laser transmission measurements are carried out at a repetition rate of 60 Hz and fluences $H \leq 10$ mJ cm^{-2} $pulse^{-1}$. The energy of each single laser pulse is recorded simultaneously in front of the sample using a beam splitter (E_{in}) and directly behind the sample (E_{out}) by fast pyroelectric detectors (PE-25H, OPHIR Optronics, Inc.) which are calibrated by the supplier for 193 nm relative to a NIST traceable standard. The ratios E_{out}/E_{in} of up to 150 consecutive laser pulses are averaged to obtain T with an absolute transmission accuracy $\Delta T \leq \pm$ 0.2 %. For each fluence H_i of the measurement sequence $H_1 \rightarrow H_2 \rightarrow H_3 \rightarrow H_1$ ($H_1 < H_2 < H_3$) the irradiation is continued until T = constant is achieved. The mean value of the last 1000...2000 transmission data is defined as the fluence dependent steady state transmission $T^{st}(H)$.

For laser induced fluorescence (LIF) measurements the samples are pre-irradiated to assure that the rapid damage process has finished. Then the repetition rate is switched to 10 Hz at constant fluence. The fluorescence light from the sample is guided by an optical fiber onto the imaging spectrograph (ISP-150, S&I GmbH, grating: 150 lines/mm)[2] and detected by an intensified, gated optical multichannel analyzer (OMA) system (ICCD-512EFT/S, S&I GmbH). Scattered laser light is shielded from the detection system by an interference filter in front of the fiber entrance with strong suppression at λ = 193 nm. The LIF signals of up to 100 consecutive laser pulses are accumulated to record one fluorescence spectrum with an enhanced signal-to-noise ratio.

Pulse energy dependent femtosecond transmission measurements are carried out at the wavelength 197 nm using the fourth harmonic of a Ti:Sa oscillator-amplifier system (oscillator: Mira 900, Coherent Inc.; amplifier: Titan, Quantronix) operating at 50 Hz repetition rate. The fs-laser pulses show in good approximation a Gaussian distribution, temporally and spatially, with a pulse width τ_{FWHM} = 350 fs and a $1/e^2$ diameter D = 51 µm. The energy of each single laser pulse is recorded simultaneously in front of the sample using a beam splitter (E_{in}) and directly behind the sample (E_{out}) by fast pyroelectric detectors. For femtosecond DUV transmission measurements 5 CaF_2 samples (30 x 30 x 15 mm^3) with different intensities of the characteristic fluorescence emission of M_{Na} centers at 620 and 740 nm are chosen. The samples are cut from the same crystals as those investigated at nanosecond ArF laser pulses. Additionally, pump-and-probe measurements using the fundamental and the second harmonic of the Ti:Sa laser at 785 nm (130 fs) and at 392 nm (220 fs), respectively, are carried out to investigate particular relaxation processes after excitation of M_{Na} centers (Fig. 2).

Here, the M_{Na} centers are excited by the second harmonic at 392 nm and the relaxation to the M_{Na} fluorescence state is analyzed by using the fundamental wavelength at 785 nm for stimulated emission depletion of the M_{Na} fluorescence state. The fluorescence signal is detected by a photomultiplier tube (H6780-20, Hamamatsu) and an interference filter is applied to block scattered laser light.

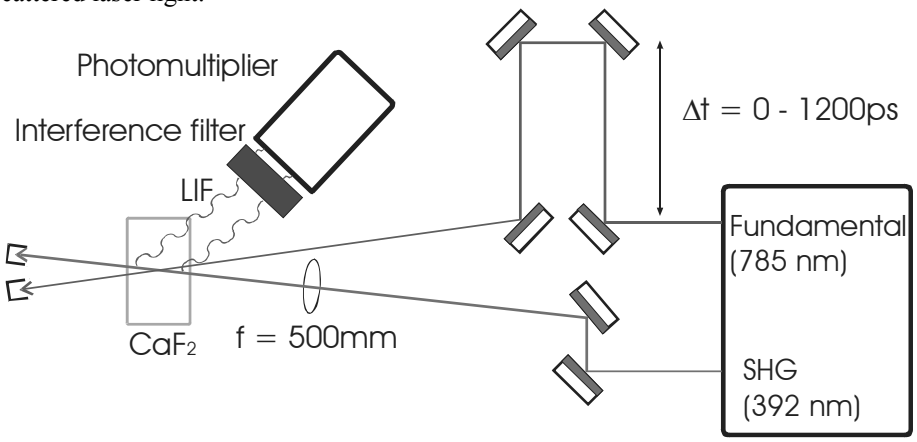

Figure 2: Schematic view of the pump-and-probe experiment to investigate particular relaxation processes

Finally, a laser induced deflection (LID) setup[11,12] (DE 101 39 906, SCHOTT AG) with enhanced sensitivity (Fig. 3) is applied to directly and absolutely measure the absorption in two CaF_2 samples (25 x 25 x 100 mm^3) at 193 nm ArF laser pulses (ExiStar Industrial, $\tau_L \approx 20$ ns, repetition rate: 1 kHz) in the fluence range 1…5 mJ cm^{-2} $pulse^{-1}$. The LID absorption measurement technique (pump-and-probe configuration) allows investigating the CaF_2 bulk absorption without any influences of the surfaces by using only small samples (typically 20 x 20 x 20 mm^3). Therefore, in upcoming experiments the typical drawbacks of DUV transmission measurements (long sample size, influence of surface quality, no distinguishing between absorption and scattering) can be overcome.

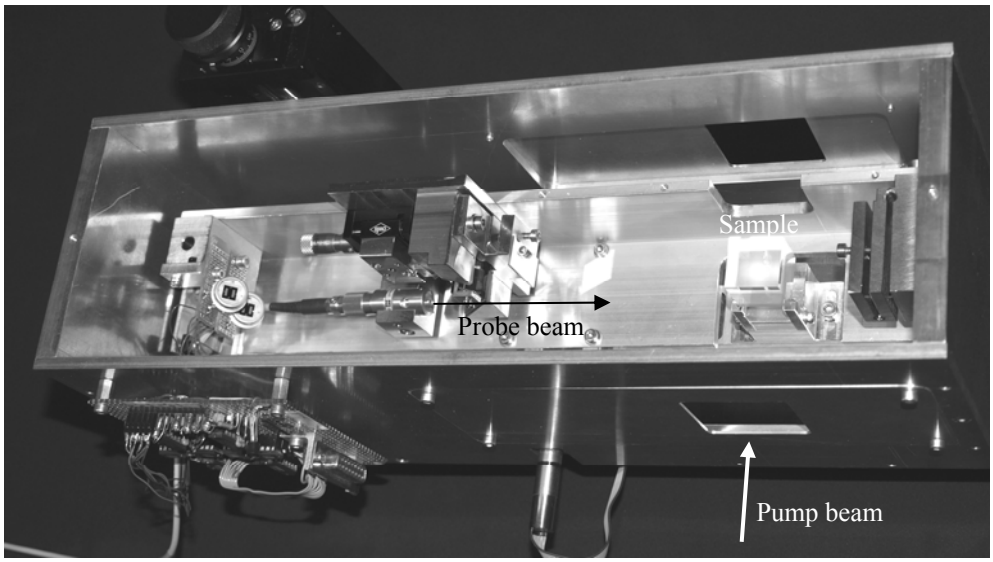

Figure 3: Sensitivity enhanced setup for direct and absolute absorption measurements using the laser induced deflection technique (LID)

3. EXPERIMENTAL RESULTS

3.1 Nanosecond transmission and fluorescence experiments at 193 nm

The measured laser pulse energy values E_{in} and E_{out} are converted to fluence values H_{in} and H_{out}, respectively. The fluence H is considered as a measure of the average laser pulse intensity I, particularly if the temporal laser beam profile

stays constant. Consequently it is very common and convenient to convert Beer´s law to $dH(z)/dz = - \alpha H(z)$ in order to describe the fluence attenuation along the sample length axis z. Keeping in mind that light scattering is very small in the highly transparent samples it appears appropriate to consider α as the absorption coefficient which is constant throughout the sample. Taking furthermore into account that the optical sample properties vary during laser irradiation and that absorption is affected by 2-photon absorption, the absorption coefficient α is described as a function of the laser pulse number N and fluence H, i.e. $\alpha = \alpha(N,H)$. Assuming that α does not depend on z, which is reasonable for weakly absorbing materials, this leads to the modified Beer´s law $dH(z)/dz = - \alpha(N,H)H(z)$. For optically thin samples, i.e. $\alpha(N,H)\, dz << 1$ and $H(z) \approx$ constant, it integrates to $\Delta H/H = - \alpha(N,H)\Delta z$. Using $|\Delta H/H| = 1 - T(N,H)/T^{max}$ the absorption coefficient is obtained by $\alpha(N,H) = (1 - T(N,H)/T^{max})/\Delta z$ with T^{max} being the ideal laser pulse transmission without any absorption or scattering by the sample but Fresnel reflection at the beam entrance and exit surfaces.
For CaF_2 samples the typical development of $\alpha(N,H)$ during the measurement sequence $H_1 \rightarrow H_2 \rightarrow H_3 \rightarrow H_1$ has been reported earlier[2,3]. The $\alpha(N,H)$ values increases/decreases throughout a series of laser pulses and for each H_i value reaches a steady state absorption coefficient $\alpha^{st}(H_i)$ which is independent from the irradiation history for the total pulse numbers applied in this work. For each sample the $\alpha^{st}(H)$ values can be expressed by a linear function $\alpha^{st}(H) = \alpha^{eff}+(\beta^{eff}/\tau_L)\, H$ (Fig. 4). Here, α^{eff} and β^{eff} are the effective 1- and 2-photon absorption coefficients, respectively, and τ_L is the laser pulse duration.

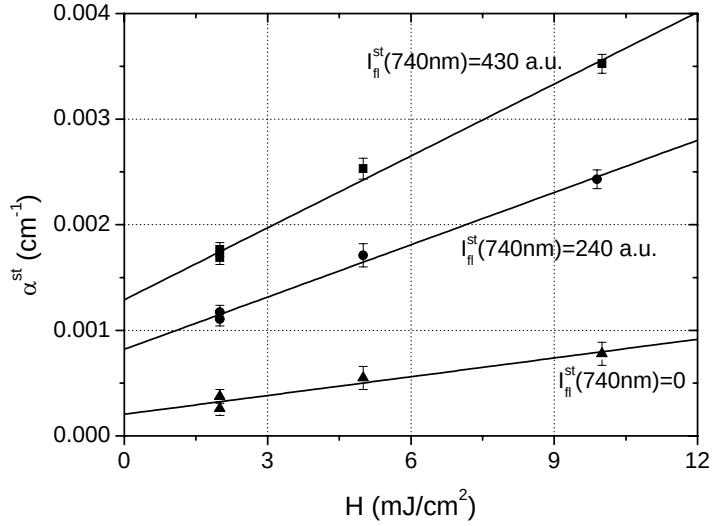

Figure 4: Comparison of $\alpha^{st}(H)$ values with their linear fits for three samples showing different fluorescence intensities $I_{fl}^{st}(740nm)$

Figure 4 and table 1 demonstrate that both, α^{eff} and β^{eff}, increase from sample to sample if their fluorescence intensity $I_{fl}(740nm)$ of the M_{Na} center emission increases. For samples showing very similar intensities $I_{fl}(740nm)$ Table 1 displays the mean of their α^{eff} and β^{eff} values. Overall α^{eff} values in the range $(2.4...16.8)x10^{-4}$ cm^{-1} and β^{eff} values in the range $(1.7...9.3)x10^{-9}$ cm W^{-1} are found. It is pointed out that samples of the highest purity ($I_{fl} \sim 0$) show the lowest α^{eff} and β^{eff} values.
Since the emission at 740 nm is an indicator of the M_{Na} center density, additional fluorescence investigations are carried out. The development of the M_{Na} center emission at 740 nm with the laser pulse number N is shown in Fig. 5 for H = 10 mJ cm^{-2} $pulse^{-1}$. The emission intensity rises with the pulse number and reaches a steady state value after about $4 \cdot 10^3$ laser pulses. For comparison the $\alpha(N,H)$ development at the same fluence H is added to Fig. 5. This comparison demonstrates, that fast absorption changes in CaF_2 upon ArF laser irradiation (= rapid damage) are related to extrinsic defects and therefore do not represent an intrinsic CaF_2 property.
The results in Fig. 6 show that the steady state fluorescence intensity $I_{fl}^{st}(740nm)$ increases linearly with the laser fluence $H \leq 20$ mJ cm^{-2} $pulse^{-1}$.

Table 1: Values α^{eff}, β^{eff} and I_{fl}^{st}(740nm) for CaF_2 (* mean values of samples showing very similar I_{fl}^{st})

I_{Fl}^{st}(740nm) [a.u.]	α^{eff} [10^{-4} cm^{-1}]	β^{eff} [10^{-9} $cm \cdot W^{-1}$]
0*	2.4 ± 1.4	1.7 ± 0.25
55*	5.7 ± 1.4	3.45 ± 0.4
65*	7.1 ± 1.3	3.8 ± 0.6
85	10 ± 0.6	4.2 ± 0.3
110*	6.0 ± 2.9	4.55 ± 0.7
150*	10 ± 5.0	4.8 ± 0.5
210*	9.3 ± 4.0	5.2 ± 0.5
240*	8.0 ± 0.7	4.8 ± 0.6
280*	9.8 ± 6.4	5.6 ± 0.5
430*	10.5 ± 2.5	6.7 ± 0.4
760	12.6 ± 0.8	7.8 ± 0.4
830	13.9 ± 0.6	8.3 ± 0.35
1110	16.8 ± 0.5	9.3 ± 0.5

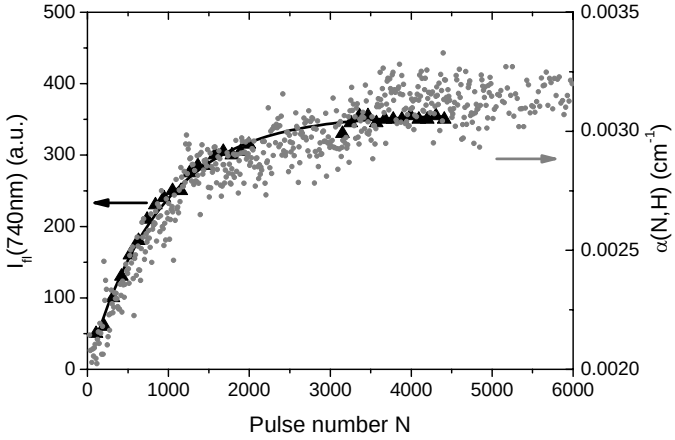

Figure 5: Intensity of the 740 nm emission I_{fl}(740nm) and the absorption coefficient α(N,H) as function of pulse number N for a Na containing CaF_2 sample at H = 10 mJ cm^{-2} $pulse^{-1}$.

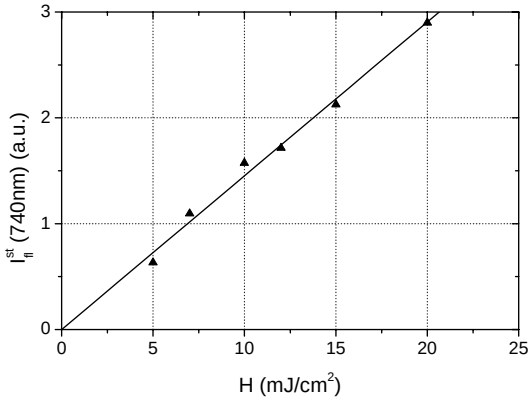

Figure 6: Dependence of the steady state fluorescence intensity I_{fl}^{st}(740nm) on the laser fluence H with linear data fit I_{fl}^{st}(H)

3.2 Nanosecond direct absorption measurements at 193 nm using LID technique

Typically, applying transmission experiments to optical materials of highest transmission suffers from various drawbacks. In order to obtain sufficient measurement accuracy long sample lengths are required (e.g. 100 mm). Furthermore, even for those long sample sizes the impact of varying surface qualities can not be neglected, especially when looking at 1-photon related loss mechanisms (1-photon absorption, scattering). Finally, transmission measurements are not able to separate between scattering and absorption. In order to overcome these drawbacks direct absorption and scattering measurement techniques have been developed throughout the last years. In order to measure the ArF laser absorption in high purity CaF_2 down to the fluence level ≤ 5 mJ cm^{-2} pulse^{-1}, we have enhanced the sensitivity of our setup based on the laser induced deflection technique (LID)[10,12]. Figure 7 shows the first measurements for high purity CaF_2 at 193 nm applying a fluence range of 1…5 mJ cm^{-2} pulse^{-1}. The resulting 2-photon absorption coefficients of 1.7x10^{-9} cm W^{-1} and 1.75x10^{-9} cm W^{-1} agree very well with the data in table 1 for CaF_2 of highest purity.

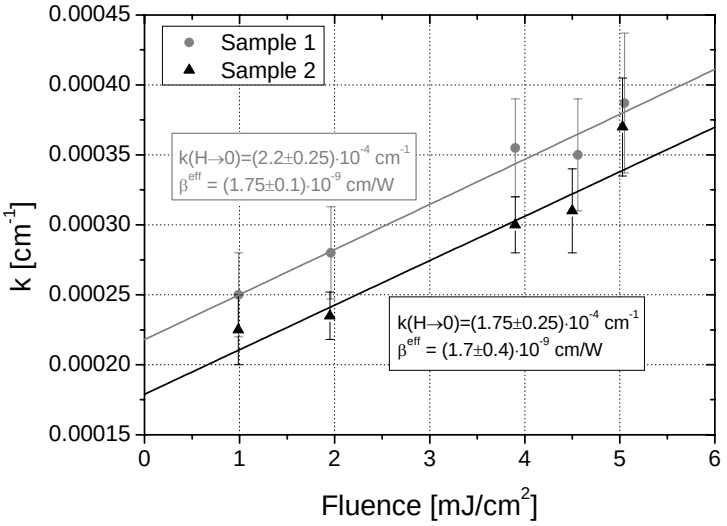

Figure 7: Results of direct absorption measurements at 193 nm of two different high purity CaF_2 samples

3.3 Femtosecond experiments at 197 nm

Due to low pulse energies (µJ range) and the very short pulse widths, 1-photon absorption processes are typically negligible compared to nonlinear absorption processes (here: 2-photon absorption) in the analysis of femtosecond transmission measurements. Therefore, the transmission of a femtosecond laser pulse through a transparent material due to the 2-photon absorption T_{TPA} is described by

$$T_{TPA} = \frac{1}{E_0} \int_{-\infty}^{\infty} \int_{A} \frac{I(t,x,y)}{1+\beta^{eff} z I(t,x,y)} dA\, dt \tag{1}$$

where E_0 is the incident energy, I(t,x,y) the temporal and spatial intensity distribution, β^{eff} the effective 2-photon absorption coefficient and z the sample length. For our experiments I(t,x,y) can be assumed Gaussian with good approximation and Equ. 1 is solved numerically. Finally, the transmission T_{TPA} is plotted against the dimension less parameter

$$x = \frac{\beta^{eff} \cdot z \cdot E_0}{\pi \cdot \tau_{FWHM} \cdot D_{1/e^2}^2} \tag{2}$$

using the pulse width τ_{FWHM} and the 1/e2 diameter $D_{1/e2}$. For the analysis the T_{TPA} value for a particular incident energy E_0 is taken from the measurement (e.g. Fig. 8b) and using that T_{TPA} value the dimension less parameter is determined from the solution of Equ. 1 (Fig. 8a). Now, with the knowledge of the laser pulse parameters and the sample length the 2-photon absorption coefficient β^{eff} is calculated.

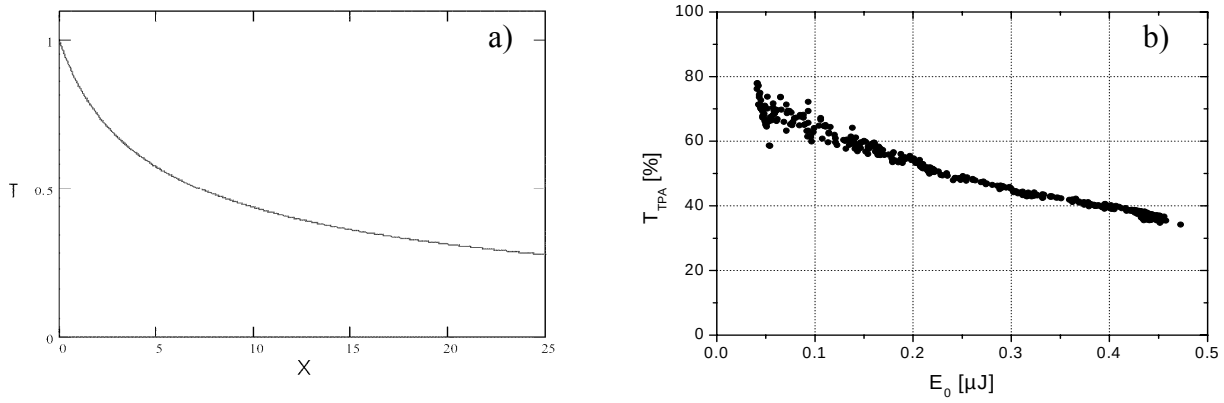

Figure 8: a) Solution of Equ. 1 for a Gaussian shaped laser pulse using the dimensionless parameter x (Equ. 2) and b) measured transmission for a CaF_2 sample showing an intensity of the M_{Na} fluorescence of I_{fl}^{st}(740nm) = 830 a.u.

Table 2 shows the comparison between the 2-photon absorption coefficients obtained by 193nm nanosecond and 197 nm femtosecond laser pulses for 5 CaF_2 samples with different M_{Na} concentrations. There are two remarkable findings: In contrast to the results for nanosecond pulses the 2-photon absorption coefficients obtained by femtosecond pulses do not show any dependence on the M_{Na} concentration identified by the characteristic fluorescence at 740 nm. Furthermore, the absolute β^{eff} values obtained for femtosecond pulses are about a factor 3 lower than the value obtained for nanosecond pulse widths and CaF_2 of highest purity ($I_{fl}^{st} = 0$).

3.4 Femtosecond pump-and-probe measurements at 392 nm and 785 nm

In order to get some more information about particular relaxation processes after excitation of M_{Na} centers, pump-and-probe measurements using the fundamental (785 nm, 130 fs) and the second harmonic (392 nm, 220 fs) of a Ti:Sa laser have been carried out (Fig. 9). Prior to the experiment a selected CaF_2 sample has been irradiated at 193 nm using nanosecond laser pulses to generate a sufficient number of M_{Na} centers. Then, the sample is "pumped" by the second harmonic at 392 nm, which is within an absorption band of the M_{Na} centers[5] and the fluorescence at 740 nm is measured. To estimate the relaxation rate k_6 (Fig. 9a), the fundamental at 785 nm is used as "probe" beam for stimulated emission depletion of the fluorescence state M_{Na}^*. The measured (spontaneous) fluorescence intensity now drops for delays between pump and probe pulse larger than $1/k_6$ when stimulated emission depletion of the fluorescence state starts. Figure 9b shows the experimental results and the relaxation time $1/k_6$ is estimated to 4 ps.

Table 2: Summary of 2-photon absorption coefficients obtained by nanosecond laser pulses at 193 nm and femtosecond laser pulses at 197 nm for 5 CaF_2 samples with different M_{Na} concentration identified by the characteristic fluorescence at 740 nm

I_{fl}^{st} (740 nm) [a.u.]	β^{eff} for τ_L ~ 30 ns [10^{-9} cm/W]	β^{eff} for τ_L ~ 350 fs [10^{-10} cm/W]
0	(1.65 ± 0.35)	(6.4 ± 1.2)
230	(4.6 ± 0.4)	(5.15 ± 1.0)
408	(6.6 ± 0.55)	(5.4 ± 1.1)
830	(8.3 ± 0.35)	(5.65 ± 1.1)
1100	(9.3 ± 0.5)	(6.0 ± 1.2)

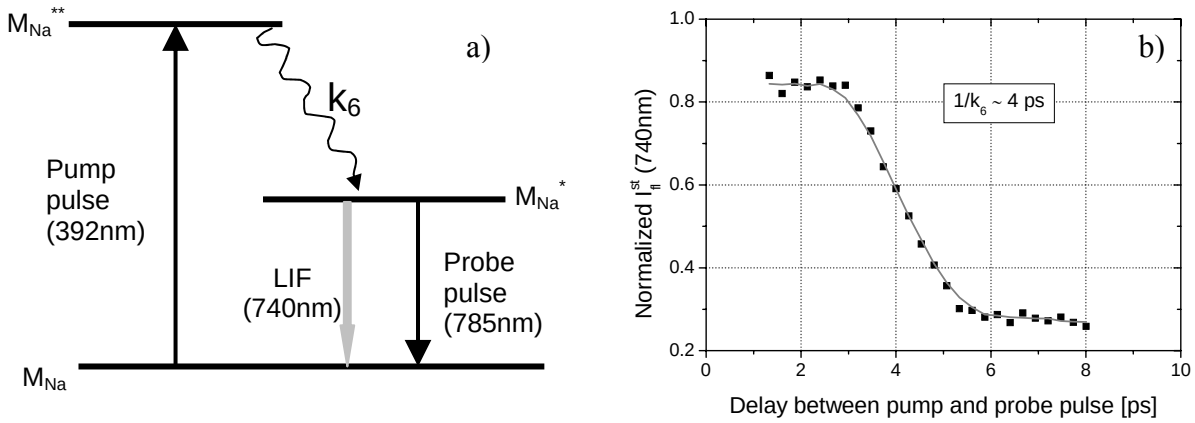

Figure 9: a) Scheme of the pump-and-probe experiment to investigate the relaxation process after excitation of M_{Na} centers (cf. text) and b) results of the pump-and-probe experiment indicating a relaxation time $1/k_6$ of about 4 ps

4. MODEL FOR THE GENERATION AND ANNEALING OF M_{NA} CENTERS

Single photon absorption by CaF_2 in the DUV spectral region can only be attributed to intrinsic and extrinsic defects because the photon energy $h\nu = 6.4$ eV is much smaller than the band gap energy $E_{gap} = 11.5…12.1$ eV of CaF_2[13,14]. Two of the most important intrinsic defects in virgin (non-irradiated) samples are the F and M centers[15,16] (F center = fluorine vacancy occupied by an electron, M center = agglomerate of two F centers) which can be stabilized by impurities like alkali metal or oxygen ions forming impurity related F_A and M_A centers with characteristic absorption and fluorescence spectra[5,8,9]. The focus of this paper lies on Na^+ stabilized F_{Na} and $M_{Na} = F + F_{Na}$ centers and their absorption around 193 nm. A model of the ArF laser induced generation and annealing of M_{Na} centers is sketched out in Fig. 10 and applied to discuss the above experimental results.

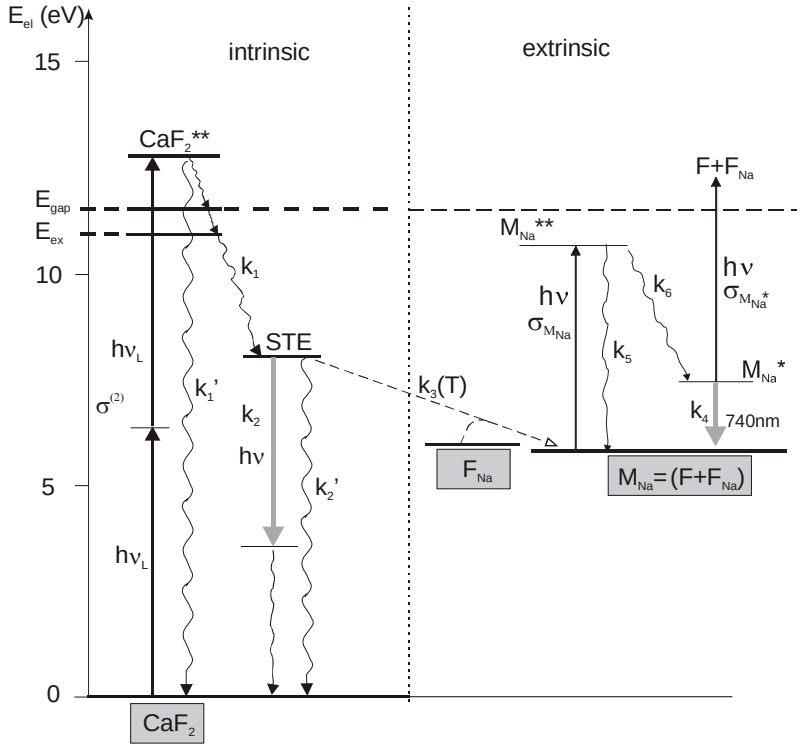

Figure 10: Scheme of the ArF laser induced generation and annealing of M_{Na} centers in CaF_2

4.1 Generation of M_{Na} centers

Virgin, Na^+ containing CaF_2 disposes initial densities of F_{Na} and M_{Na} centers from its production and prior to ArF laser irradiation. The ArF laser induced M_{Na} generation essentially originates from highly excited CaF_2^{**} obtained by intrinsic 2-photon absorption in CaF_2 (Fig. 10) creating pairs of free electrons and holes (H). A large part of these pairs will rapidly form self-trapped excitons (STE)[15] by the rate constant $k_1 = 10^{12}$ s^{-1} via the mobile exciton (pair of F+H) at E_{ex} without specifying details of the relaxation route[17] (k_1' << k_1 due to relatively inefficient electron-phonon coupling for the large energy gap E_{gap} = 11.5…12.1 eV). STE relaxation ($k_{STE} = k_2 + k_2' + k_3(T)\,[F_{Na}]$) follows the well known emission route (λ = 278 nm, $k_2 = 1/\tau_{fl}(278nm) \sim 10^6$ s^{-1}) with subsequent radiationless deactivation to ground state CaF_2 and two radiationless processes (k_2', $k_3(T)\,[F_{Na}]$). The purely radiationless deactivation of STE to CaF_2 (k_2') is considered negligible for equivalent reasons as in the k_1 vs. k_1' case. The H center of the STE can diffuse away from the F center by thermal activation (E_a = 0.4 eV)[18] and the remaining F center may form M_{Na} centers via $F + F_{Na} \rightarrow M_{Na}$. This diffusion of the H center from the F center of the STE is the rate determining step of the rate constant $k_3(T)$.
For ArF laser pulse durations $\tau_L \approx 30$ ns and the high $k_1 = 10^{12}$ s^{-1} value, STE generation occurs during the ArF laser pulses only and the STE density at the end of the laser pulse is calculated to be $[STE](\tau_L) = \sigma^{(2)}\,[CaF_2]\,I^2\,\tau_L$ with $\sigma^{(2)}$ being CaF_2's intrinsic two photon absorption cross section. Due to the low k_2 value and its independence from the Na concentration the M_{Na} generation from STE takes dominantly place in the dark period τ_{dp} between the laser pulses. Thus, simplified rate equations are valid for the developments [STE](t) and $[M_{Na}](t)$ within τ_{dp}:

$$d[STE](t)/ = -(k_2+k_3(T)\,[F_{Na}])\,[STE](t) \quad (3)$$

$$d[M_{Na}](t)/dt = k_3(T)\,[F_{Na}]\,[STE](t) \quad (4)$$

For high initial F_{Na} center concentrations F_{Na} is considered large compared to any changes during M_{Na} center formation ($[F_{Na}] \approx [F_{Na}](initial) = constant$). Thus, rate equation 3 can be solved and the result inserted into Eq. 4 (taking into account $(k_2+k_3[T]\,[F_{Na}]) >> 1/\tau_{dp}$) yielding the laser induced M_{Na} concentration generated during a single dark period τ_{dp}

$$[M_{Na}](\tau_{dp}) = \left(\frac{k_3(T)[F_{Na}]}{k_2 + k_3(T)[F_{Na}]}\right)\sigma^{(2)}\,[CaF_2]\,I^2\,\tau_L = \left(\frac{k_3(T)[F_{Na}]}{k_2 + k_3(T)[F_{Na}]}\right)STE(\tau_L). \quad (5)$$

4.2 Annealing of M_{Na} centers

Annealing of M_{Na} centers can occur by its dissociation into a pair of F and F_{Na} centers. Dissociation is assumed to follow two subsequent 1-photon absorption steps during a single nanosecond laser pulse. Firstly, a highly excited state M_{Na}^{**} is populated which quickly relaxes (k_6) to the fluorescent state M_{Na}^{*}. The M_{Na}^{*} state is depopulated either by fluorescence emission (k_4) to the M_{Na} ground state or by fast photo dissociation into a pair of F and F_{Na} centers after further single photon absorption ($\sigma_{MNa^*} \cdot I$). Thus, in contrast to its generation, M_{Na} annealing takes place during the laser pulse. The associated simplified rate equations for laser pulse number N are:

$$d[M_{Na}](t)/dt \approx 0 \quad (6)$$

$$d[M_{Na}^{**}](t)/dt = \sigma_{MNa}\,[M_{Na}]_N(0)\,I - (k_5+k_6)\,[M_{Na}^{**}](t) \quad (7)$$

$$d[M_{Na}^{*}](t)/dt = k_6\,[M_{Na}^{**}](t) - (k_4+\sigma_{MNa^*}\,I)\,[M_{Na}^{*}](t) \quad (8)$$

$$d[F+F_{Na}]/d\,t = \sigma_{MNa^*}\,I\,[M_{Na}^{*}](t) \quad (9)$$

Equation 6 takes into account that the change of $[M_{Na}]$ by 1-photon absorption within one laser pulse is negligible for the calculations of Eq. 7 ($[M_{Na}] \approx [M_{Na}]_N(0)$; $[M_{Na}]_N(0) = M_{Na}$ density at the onset of laser pulse N). For solving rate equations 7 and 8, it is taken into account that $(k_5+k_6) >> 1/\tau_L$ (no delay between laser pulse and fluorescence at 740 nm) and $(k_4+\sigma_{MNa^*}\,I) > 1/\tau_L$. As a result the population of the fluorescent state M_{Na}^{*} at the end of laser pulse N is obtained. Inserting the solution of $[M_{Na}^{*}](t)$ into Eq. 9 and integrating over the laser pulse duration τ_L yields the density decrease of M_{Na} centers by photo dissociation and the remaining M_{Na} density $[M_{Na}]_N(\tau_L) = [M_{Na}]_N(0) - [F+F_{Na}](\tau_L)$ at the end of laser pulse N:

$$[M_{Na}]_N(\tau_L) = [M_{Na}]_N(0)\left[1 - \sigma_{M_{Na}}\sigma_{M_{Na}^*}\,I^2\left(\frac{k_6}{k_6+k_5}\right)\left(\frac{\tau_L}{k_4+\sigma_{M_{Na}^*}\,I}\right)\right] = [M_{Na}]_N(0)\,\varepsilon, \quad \varepsilon < 1. \quad (10)$$

4.3 Model results

For a large laser pulse series at constant fluence H and intermediate dark periods τ_{dp} the steady state density M_{Na} density is calculated by a geometric series to be

$$[M_{Na}]^{st} = \left(\frac{k_6 + k_5}{k_6}\right)\left(\frac{k_3(T)[F_{Na}]}{k_2 + k_3(T)[F_{Na}]}\right)\frac{\sigma^{(2)}}{\sigma_{M_{Na}}\sigma_{M^*_{Na}}}[CaF_2]\left(k_4 + \sigma_{M^*_{Na}} I\right). \tag{11}$$

The steady state population of the fluorescent state M_{Na}^* is now obtained

$$[M_{Na}{}^*]^{st} = \left(\frac{k_3(T)[F_{Na}]}{k_2 + k_3(T)[F_{Na}]}\right)\frac{\sigma^{(2)}}{\sigma_{M^*_{Na}}}[CaF_2]\, I \cdot \tag{12}$$

The additional contributions of the M_{Na} center to the steady state absorption coefficient $\alpha^{st}(H=I\,\tau_L)$ originate from both, the absorption $\alpha^{st}_{M_{Na}}(H)$ from its ground state M_{Na} and from absorption $\alpha^{st}_{M^*_{Na}}(H)$ from its fluorescent state M_{Na}^* where $\beta^{int} = \sigma^{(2)}$ $[CaF_2]$ is the intrinsic two-photon absorption coefficient of CaF_2. For CaF_2 samples containing M_{Na} centers the effective 1- and 2-photon absorption coefficients α^{eff} and β^{eff} are now expanded to $\alpha^{eff}=\alpha^{int}+\alpha^{add}$ and $\beta^{eff}=\beta^{int}+\beta^{add}$. α^{int} and β^{int} are the intrinsic values of highest purity CaF_2 whereas α^{add} and β^{add} result from the Na related M_{Na} centers with

$$\alpha^{add} = \left(\frac{k_3(T)[F_{Na}]}{k_2 + k_3(T)[F_{Na}]}\right)\left(\frac{k_6 + k_5}{k_6}\right)\frac{\beta^{\text{int}}}{\sigma_{M^*_{Na}}}k_4; \qquad \beta^{add} = \left(\frac{k_3(T)[F_{Na}]}{k_2 + k_3(T)[F_{Na}]}\right)\left(1 + \frac{k_6 + k_5}{k_6}\right)\beta^{\text{int}}. \tag{13}$$

5. DISCUSSIONS

5.1 Effective absorption coefficients α_{eff} and β_{eff} (nanosecond laser pulses)

Both, α^{eff} and β^{eff}, increase with increasing 740nm fluorescence emission (Table 1; Figs. 3 and 5). To separate α^{eff} and β^{eff} into their intrinsic contributions α^{int} and β^{int} and their Na-related additive contributions α^{add} and β^{add}, the intrinsic contributions are derived from the high purity CaF_2 sample ($\alpha^{eff}=(2.4\pm1.4)\text{x}10^{-4}$ cm^{-1}, $\beta^{eff}=(1.7\pm0.25)\text{x}10^{-9}$ cm W^{-1}). The β^{int} value agrees very well with the value $(2 \pm 1)\text{x}10^{-9}$ cm W^{-1} reported for the intrinsic 2-photon absorption in CaF_2[19]. The additional contributions α^{add} and β^{add} are explained by the rate equation model showing steady state absorption by the M_{Na} centers (Eq. 13). The linear contribution appears trivial (Fig. 10). The nonlinear contribution by M_{Na} is not straightforward, as the only 2-photon absorption process occurs in CaF_2 itself ($CaF_2^{**} \leftarrow CaF_2$). The fluence (intensity) dependent steady state M_{Na}^{st} density, however, causes a M_{Na}-related contribution to β^{eff}. To further check the consistency of the model with the experimental findings, the β^{add} values are plotted against the α^{add} values (Fig. 11). Within the error limits a linear relation between β^{add} and α^{add} is found as can be expected from Eq. 13:

$$\frac{\beta^{add}}{\alpha^{add}} = \frac{\sigma_{M^*_{Na}}}{k_4}\left(1 + \frac{k_6}{k_6 + k_5}\right). \tag{14}$$

5.2 M_{Na} defect center emission at 740 nm

The M_{Na} emission at 740 nm reflects the population of the fluorescent state M_{Na}^* and thereby also the population of the M_{Na} ground state. Since both states contribute to the additional absorption α^{add} in Na containing CaF_2, the emission at 740 nm and the absorption at 193 nm should both follow the ArF laser induced M_{Na} center kinetics and depend on the number of laser pulses N. This is validated by the results shown in Fig. 5.

In steady state condition the I_{fl}^{st}(740 nm) values should obey a linear dependence on the applied laser intensity I (fluence H) according to Eq. 12 since I_{fl}^{st}(740 nm) ∝ $[M_{Na}^{*}]^{st}$. This is shown by the linear fit of the experimental data in Fig. 6 up to H=20 mJcm^{-2}pulse^{-1}.

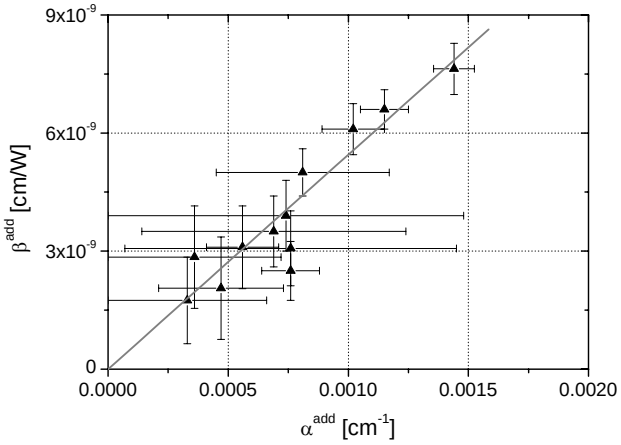

Figure 11: Na-related 2-photon absorption β^{add} vs. Na-related 1-photon absorption α^{add} of CaF_2 samples showing 740 nm emission of M_{Na} centers (cf. text)

5.3 Effective 2-photon absorption coefficients β^{eff} (femtosecond laser pulses)

In contrast to the results for nanosecond laser pulse, no additional 2-photon absorption coefficient β^{add} is found in Na containing CaF_2 when applying 197 nm pulses of 350 fs width. Thus, all investigated samples, despite their large difference in the M_{Na} concentration, show practically the same β^{eff} values. This result is also explained by applying the introduced model for M_{Na} center generation and annealing taking into account that the relaxation from the excited state M_{Na}^{**} to the fluorescent state M_{Na}^{*} (k_6) takes about 4 ps (Fig. 9). Thus, the laser pulse width (350 fs) is too short to allow M_{Na} dissociation via 1-photon absorption from the fluorescent state M_{Na}^{*} ($\sigma_{MNa*} \cdot I$) within a single laser pulse. Since the lifetime of the M_{Na}^{*} state is much smaller than the time between consecutive laser pulses[2], i.e. all M_{Na} centers are in ground state at the start of the next pulse, no M_{Na} center annealing occurs for the applied pulse width of 350 fs. As a result, the M_{Na} center can only act as 1-photon absorber and does not influence the effective 2-photon absorption coefficient β^{eff}.

The absolute and practically constant β^{eff} values of the measured CaF_2 samples are about a factor of 3 below the lowest value found for high purity CaF_2 and nanosecond pulses. The authors assume that for pulse widths shorter than the STE formation time (~1ps), no (intrinsic) two-step absorption via intermediate STE energy states can occur during pulse duration. In contrast, nanosecond laser pulses are long compared to the STE formation time and 2-photon absorption consists of two intrinsic parts, the simultaneous absorption of two photons and the two-step absorption via intermediate STE energy states. To prove this assumption, further pump-and-probe experiments will be carried out.

6. SUMMARY

Sodium containing CaF_2 samples were identified by the characteristic emission at 740 nm of Na related M_{Na} centers. CaF_2 samples with Na and some highest purity samples were studied with respect to their DUV transmittance for nanosecond and femtosecond laser pulses. For nanosecond laser pulses at 193 nm the steady state α^{st}(H) values were expressed by the linear relation $\alpha^{st}(H) = \alpha^{eff}+(\beta^{eff}/\tau_L)$ H, the sample's effective 1- and 2-photon absorption coefficients α^{eff} and β^{eff}, respectively. The lowest α^{eff} and β^{eff} values were obtained with the highest purity samples and taken as the intrinsic values α^{int} and β^{int}. The values $\alpha^{add} = \alpha^{eff} - \alpha^{int}$ and $\beta^{add} = \beta^{eff} - \beta^{int}$, attributed to the Na related 1- and 2-photon absorption, increases with increasing Na concentration. For femtosecond laser pulses at 197 nm the 2-photon absorption coefficient is not a function of the Na concentration. Instead, a roughly constant value β^{eff} is found that is by a factor of 3

lower than the intrinsic value β^{int} found at nanosecond pulse width for the highest purity samples. The experimental results are explained by applying a new rate equation model assuming a dynamic equilibrium of laser induced M_{Na} generation and annealing in Na containing CaF_2. M_{Na} generation is due to the intrinsic 2-photon absorption yielding self-trapped excitons (STE) followed by their thermally activated separation into F and H centers. The F centers of the STE can combine with existing Na related F_{Na} centers to form M_{Na} centers. M_{Na} annealing occurs by its dissociation into a pair of $F+F_{Na}$ after two consecutive 1-photon absorption processes into a highly excited M_{Na} state. The different results for nanosecond and femtosecond pulses are related to formation and relaxation processes that are fast compared to nanosecond but slow compared to femtosecond pulse durations.

ACKNOWLEDGEMENTS

The authors thank the Schott-Jenaer-Glas-Fonds for financial support and are grateful to SCHOTT AG / Division SCHOTT LITHOTEC, Jena. Its co-workers kindly provided the CaF_2 samples and gave many useful hints during fruitful discussions.

REFERENCES

[1] Bödefeld, R., Koerner, J., Siebold, M., Wolf, M., Herrmann, A., Hein, J. and Kaluza, M.C., "Comparative damage study on ytterbium-doped materials for diode-pumped high energy lasers," Proc. SPIE 7132, 7132 14 (2008).
[2] Mühlig, Ch., Triebel, W., Töpfer, G. and Jordanov, A., "Calcium fluoride for ArF laser lithography – characterization by in situ transmission and LIF measurements," Proc. SPIE 4932, 458-466 (2002).
[3] Mühlig, Ch., Triebel, W., Töpfer, G., Bergmann, J., Brückner, S., Chojetzki, Ch. and Martin, R., "Laser induced fluorescence of calcium fluoride upon 193 nm and 157 nm excitation," Proc. SPIE 5188, 123-133 (2003).
[4] Burkert, A., Mühlig, Ch., Triebel, W., Keutel, D., Natura, U., Parthier, L., Gliech, S., Schröder, S. and Duparré, A., "Investigating the ArF laser stability of CaF_2 at elevated fluences," Proc. SPIE 5878, 14-21 (2005).
[5] Komine, N., Sakuma, S., Shiozawa, M., Mizugaki, T. and Sato, E., "Influence of sodium impurities on ArF excimer-laser-induced absorption in CaF_2 crystals," Appl. Opt. 39, 3925-3930 (2000).
[6] Mizuguchi, M., Hosono, H., Kawazoe, H. and Ogawa, T., "Generation of optical absorption bands in CaF_2 single crystals by ArF excimer laser irradiation: Effect of yttrium impurity," J. Vac. Sci. Technol. A 16, 3052-3057 (1998).
[7] Mizuguchi, M., Hosono, H., Kawazoe, H. and Ogawa, T., "Time-resolved photoluminescence for diagnosis of resistance to ArF excimer laser damage to CaF_2 single crystals," J. Opt. Soc. Am. B 16, 1153-1159 (1999).
[8] Rauch, R. and Schwotzer, G., "Disturbed colour centres in oxygen- and alkali-doped alkaline earth fluoride crystals after X-ray irradiation," phys. stat. sol. (a) 74, 123-131 (1982).
[9] Arkhangel'skaya, V.A., Reiterov, V.M., Trofimova, L.M. and Shcheulin, A.S., "Optical properties of Fluorite-type crystals with M_A color centers," Zhurnal Prikladnoi Spektroskopii 37, 644-648 (1982)
[10] Mühlig, Ch., Kufert, S., Triebel, W. and Coriand, F., "Simultaneous measurement of bulk absorption and fluorescence in fused silica upon ArF laser irradiation," Proc. SPIE 4779, 107-116 (2002).
[11] Guntau, M. and Triebel, W., "A Novel Method to Measure Bulk Absorption in Optically Transparent Materials," Rev. Sci. Instr. 71, 2279-2282 (2000).
[12] Mühlig, Ch., Triebel, W., Kufert, S. and Bublitz, S., "Characterization of low losses in optical thin films and materials," Appl. Opt. 47, C135-C142 (2008).
[13] Rubloff, G.W., "Far-Ultraviolet Reflectance Spectra and the Electronic Structure of Ionic Crystals," Phys. Rev. B 5, 662-684 (1972).
[14] Tomiki, T. and Miyata, T., "Optical studies of alkali fluorides and alkaline earth fluorides in VUV region," J. Phys. Soc. Jap. 27, 658-678 (1969).
[15] Williams, R.T., "Optically generated lattice defects in halide crystals," Optical Engineering 28, 1024-1033 (1989).
[16] Letz, M. and Parthier, L., "Charge centers in CaF_2: *Ab initio* calculation of elementary physical properties," Phys. Rev. B 74, 064116 (2006).
[17] Lindner, R., PhD thesis (Freie Universität Berlin, Germany) (2000).
[18] Rix, S. (SCHOTT AG), personal communication.
[19] Tsujibayashi, T., Toyoda, K., Sakuragi, S., Kamada, M. and Itoh, M., "Spectral profile of the two-photon absorption coefficients in CaF_2 and BaF_2," Appl. Phys. Lett. 80, 2883-2885 (2002).